Modified Wheat Straw Biochar Optimization *via* Response Surface Methodology for Cr(VI) Removal from Aqueous Solution

Hansheng Li [a,b] Ahmad Razali Ishak [a,*] Mohd Shukri Mohd Aris [a] Siti Norashikin Mohamad Shaifuddin [a] Tiantian Deng [b] and Su Ding [b]

** Corresponding author: ahmadr2772@uitm.edu.my*

DOI: 10.15376/biores.21.2.3954-3980

GRAPHICAL ABSTRACT

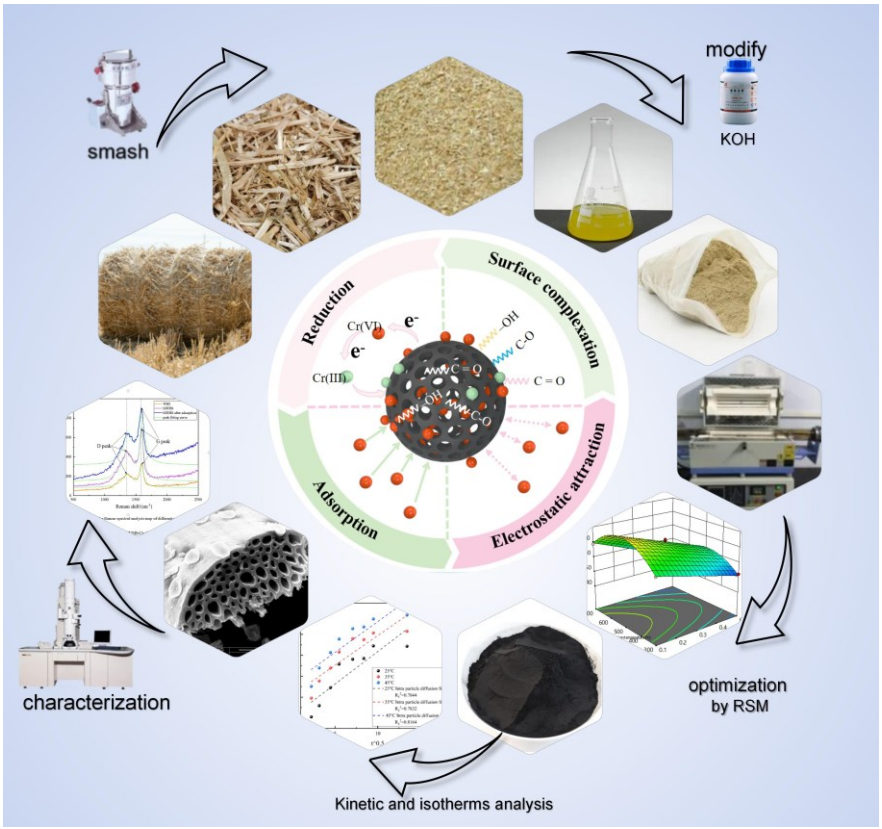

Modified Wheat Straw Biochar Optimization *via* Response Surface Methodology for Cr(VI) Removal from Aqueous Solution

Hansheng Li [a,b] Ahmad Razali Ishak [a,*] Mohd Shukri Mohd Aris [a] Siti Norashikin Mohamad Shaifuddin [a] Tiantian Deng [b] and Su Ding [b]

The preparation of wheat straw biochar (MWSB) was optimized using response surface methodology (RSM) with a Box-Behnken Design (BBD) to maximize Cr(VI) removal. Parameters assessed were wheat straw particle size, KOH modifier concentration, and pyrolysis temperature. Optimal conditions (0.1 mm particle size, 3 mol/L KOH, 494 °C pyrolysis) yielded 86.5% Cr(VI) removal efficiency. Adsorption kinetics followed the pseudo-second-order model, and isotherm data fitted the Langmuir model, indicating monolayer adsorption limited by site density. The Langmuir model gave a maximum adsorption capacity (Q_{max}) of 105.28 mg/g at 25 °C. MWSB was characterized using SEM-EDS, FTIR, Raman spectroscopy, and XPS. The optimized MWSB preparation significantly enhanced the efficacy and feasibility of wheat straw in environmental applications, particularly for Cr(VI) removal.

DOI: 10.15376/biores.21.2.3954-3980

Keywords: Wheat straw biochar; Optimization; RSM; Cr(VI); Adsorption; Characterization

*Contact information: a: Centre for Environmental Health and Safety Studies, Faculty of Health Sciences, Universiti Teknologi MARA, Puncak Alam Campus, Kuala Selangor 42300, Selangor, Malaysia; b: School of Environmental and Biological Engineering, Henan University of Engineering, Zhengzhou 451191, China; *Corresponding author: ahmadr2772@uitm.edu.my*

INTRODUCTION

Chromium in the natural world is widely distributed in the Earth's crust, primarily existing as chromite ($FeCr_2O_4$) within minerals. Chromium is an important metal pollutant, which has caused serious water pollution due to its widespread use in industries such as tanning, metallurgy, batteries, and textiles (Lin *et al.* 2018). Chromium exists primarily in water as hexavalent chromium (Cr(VI)) and trivalent chromium (Cr(III)). Among these two forms, Cr(III) serves as an essential trace element critical for human physiological functions and is relatively non-toxic. In contrast, hexavalent chromium is a highly toxic, carcinogenic, and mutagenic water pollutant that poses a severe threat to human health and the environment, thus attracting widespread attention from researchers (Altundogan 2005; Liu *et al.* 2016; Ahmad *et al.* 2022). In typical Cr(VI)-contaminated water and wastewater from electroplating, the concentration of Cr(VI) ranges between 30 to 200 $mg \cdot L^{-1}$, which is significantly higher than the World Health Organization's limit of 50 micrograms per liter (Lyu *et al.* 2017). Considering the toxicity of hexavalent chromium, it is necessary to find a green and sustainable method for removing hexavalent chromium from the aquatic environment.

The purification technologies usually used for Cr(VI)-containing sewage include precipitation, membrane filtration, amine solvent extraction, ion exchange, adsorption, electrodeposition, and other biological processes (Sinha *et al.* 2022; Jamil *et al.* 2023). Among these technologies, adsorption is a preferred method due to its advantages of being easy to handle, flexible, and efficient (Zhao *et al.* 2015; Bibi *et al.* 2018). Common adsorbents used for the adsorption of hexavalent chromium include biochar, activated carbon, clay minerals, organic polymers, and nano-metal oxides (Islam *et al.* 2019). Most adsorbents, such as activated carbon and clay minerals, are costly and difficult to recycle. Therefore, developing new types of adsorbents that are simple to synthesize, low-cost, and chemically stable has become an urgent issue to address (Bachmann *et al.* 2022).

Biochar, a structural carbon matrix characterized by high porosity and a large specific surface area, contains complex surface-active functional groups (Ali *et al.* 2020; Kapoor *et al.* 2021; Sinha *et al.* 2022; Lalmalsawmdawngliani *et al.* 2024), which allows it to be used as an adsorbent or carrier of other catalysts to remove Cr(VI) from aqueous solutions (Li *et al.* 2019; Zeng *et al.* 2021). Biochar has a wide range of sources; common agricultural and forestry wastes, such as wheat straw, bagasse, banana peels, and peanut shells, can all serve as raw materials to produce biochar. Fang *et al.* engineered nZVI@CMBC—a chicken manure-derived biochar composite loaded with nanoscale zero-valent iron—and applied it to effectively eliminate hexavalent chromium from wastewater (Fang *et al.* 2022). The results showed that under acidic conditions, the removal efficiency of the nZVI/CMBC composite for hexavalent chromium could reach 124 mg/g. Luo *et al.* engineered BC-Ce, a nanoceria-functionalized biochar derived from peanut shells, through a sequential impregnation-precipitation-pyrolysis approach, achieving simultaneous adsorption and reduction of Cr(VI) in water with a low-cost, recyclable material (Luo *et al.* 2023). The results showed that BC-Ce exhibited excellent adsorption efficacy for hexavalent chromium (Cr(VI)), with the Langmuir model calculating a maximum capacity of 47.8 mg/g. The aforementioned research has demonstrated the feasibility and advantages of utilising agricultural waste to prepare highly efficient adsorbents, providing valuable insights for the high-value utilisation of wheat straw. Wheat is the staple food grain in North China and has abundant straw resources (Zhang *et al.* 2019; Lu *et al.* 2021). Although the comprehensive utilization rate of straw is increasing each year (Wang *et al.* 2020a), there are still regional, seasonal, and structural excess phenomena (Zhang *et al.* 2019; Chen *et al.* 2020). According to statistics, between 2011 and 2022, China's annual wheat straw production increased from approximately 139 million tonnes to around 161 million tonnes (Junjie *et al.* 2025). However, a large amount of wheat straw is not effectively utilized each year. Due to the time-consuming and labor-intensive nature of straw return to fields, the phenomenon of straw burning has become increasingly common. The burning of straw releases a large amount of pollutants, leading to many environmental problems (Zhang *et al.* 2013). Using wheat straw as a raw material for the preparation of biochar is one of the effective ways to reuse it, while also reducing its negative impact on the environment. Concurrently, the elemental composition of wheat straw indicates significant potential for preparing wheat straw biochar. Carbon and oxygen constitute the primary elements in wheat straw, with carbon content accounting for approximately 40 to 50%. Although wheat straw also contains minerals such as silica and other inorganic elements naturally, the ash content of these is mostly below 10% (Jain 2026; Wang *et al.* 2021). Wheat straw-based biochar demonstrates broad application prospects in wastewater treatment (Li *et al.* 2016; Liu *et al.* 2012; Wang *et al.* 2026a), soil remediation (Ma *et al.* 2025; Wang *et al.* 2025), soil improvement (Yan *et al.* 2025; Zhong *et al.* 2025), and soil

carbon sequestration (Chang *et al.* 2025). Among these, there have been many studies on the use of wheat straw to produce biochar to control heavy metal pollution (Li *et al.* 2019; Ali *et al.* 2020; Irfan *et al.* 2021; Ćwieląg-Piasecka *et al.* 2023). However, prior research has demonstrated that raw biochar's adsorption and activation capacities are constrained by its limited specific surface area, deficient functional groups, and low graphitization levels. These issues can be effectively improved through various physical and chemical modifications (Peiris *et al.* 2017; Krasucka *et al.* 2021). Potassium hydroxide (KOH) is one of the commonly used modifiers for biochar. Because of its excellent intercalation and activation properties, KOH is widely used to enrich the porous structure of biochar, thereby increasing its specific surface area. Wang *et al.* (2023) investigated the efficacy of KOH-modified biochar in adsorbing tetracycline (TC) and Cr(VI), demonstrating its enhanced pollutant removal capabilities. The results showed that the pore characteristics and redox capacity of the biochar were improved after modification with KOH.

To the authors' knowledge, no prior studies have systematically investigated the optimization of Cr(VI) adsorption through KOH-modified wheat straw biochar (MWSB) Therefore, this study aimed to fill this gap by investigating the optimization of Cr(VI) removal using MWSB from an aqueous solution. The optimization protocol was further confirmed by analyzing the influence of critical variables, including KOH concentration, wheat straw dimensions, and thermal treatment conditions. In this study, wheat straw biochar was modified by KOH impregnation (Jamil *et al.* 2023), and then prepared by oxygen-limited temperature-controlled term pyrolysis in different temperature (Wang and Wang 2019). Based on the biochar preparation methodology, three parameters—wheat straw particle size, modifier concentration, and term pyrolysis temperature—were established as experimental variables for optimizing biochar synthesis conditions. Therefore, BBD method was used to prepare wheat straw biochar, RSM was employed to optimize the synthesis parameters of wheat straw biochar, followed by systematic investigation of Cr(VI) adsorption kinetics and equilibrium isotherm behavior. In addition, biochar has undergone several structural and chemical analysis tests such as SEM-EDS, Raman, and FTIR.

EXPERIMENTAL

Materials

The wheat straw utilized in this investigation was sourced from Zhoukou City, Henan Province, China. All chemical reagents, including $K_2Cr_2O_7$, HCl, H_2SO_4, $ZnCl_2$, H_3PO_4, $C_{13}H_{14}N_4O$, CH_3COCH_3, and KOH, were of analytical grade and procured from Tianjin Kemi Ou Reagent Co., Ltd. Ultrapure water was employed for all experimental procedures.

Sample Preparation Method

The raw wheat straw material underwent a series of processing steps, commencing with washing, followed by drying, and subsequent crushing utilizing a crusher. The particle size distribution of the wheat straw powder, featuring varying sizes, was achieved through usage of diverse screens. This powder was then immersed in KOH solutions of varying concentrations, subjected to continuous stirring for 24 h.

Subsequently, the wheat straw powder was separated through filtration, rinsed with purified water to achieve neutrality, and finally dried at 105 °C. The dried wheat straw powder was introduced into a high-temperature tube furnace, where biochar was generated using a temperature-controlled term pyrolysis method with restricted oxygen. The temperature ascended at a rate of 10 °C/min, and after 2 h, it naturally descended to room temperature. Sample is removed and stored for future use.

Experimental Methods for Chromium Adsorption

For Cr(VI) removal assays, biochar samples were introduced into 50 mL Cr(VI) solutions (50 mg/L) under pH-adjusted acidic conditions and incubated in a temperature-controlled orbital shaker (25 °C, 150 rpm) for 24 h. Post-equilibration, residual Cr(VI) concentrations in the supernatant were quantified *via* diphenylcarbazide (DPC) spectrophotometric analysis (Zhou and Sun 2002; Govindaraju *et al.* 2024).

The removal efficiency η (Eq. 1) and the equilibrium adsorption capacity Q_e (Eq. 2) (Santhosh *et al.* 2020), were confirmed to illustrate the adsorption effect. They are calculated by the following formulas:

$$\eta = \frac{(C_0 - C_e)}{C_0} \times 100\% \quad (1)$$

$$Q_e = \frac{(C_0 - C_e) \times V}{m} \quad (2)$$

where C_0 and C_e represent the initial concentration of Cr(VI) and the equilibrium concentration level at the end of the reaction, mg/L; Q_e represents the equilibrium adsorption of the reaction, mg/ g; V is the reaction volume of the Cr(VI) solution, mL; and m is the mass of the adsorbent added, g.

Optimization and Preparation of MWSB

This study implemented Response Surface Methodology (RSM) to systematically optimize biochar preparation parameters. The Cr(VI) adsorption capacity of biochar served as the response variable (Xiao *et al.* 2022). A Box-Behnken experimental design (Yavari *et al.* 2017) was adopted to optimize three critical preparation parameters including wheat straw particle size (Nartey and Zhao 2014), modifier concentration (Yu *et al.* 2024), and term pyrolysis temperature (Ameen Hezam Saeed *et al.* 2022), and the experimental factors and levels are shown in Table 1. The experimental design comprised 17 biochar variants, each synthesized and subsequently assessed for Cr(VI) adsorption performance in 50 mg/L aqueous solutions.

The experimental data were analyzed and fitted with a quadratic model using Design-Expert 13.0 software (Ashfaq *et al.* 2022), and this model helped predict the optimum preparation conditions for biochar and explored the interaction between dependent and independent factors. Analysis of variance (ANOVA) was applied to evaluate the validity of the quadratic model and statistically assess the significance of individual terms within the regression equation (Saini *et al.* 2022). Biochars synthesized under optimized preparation parameters were designated as MWSB. In parallel, the unmodified wheat straw biochar (WSB) was synthesized under the same conditions applied for the optimized MWBC preparation, facilitating a comprehensive comparative analysis of their respective physicochemical characteristics and Cr(VI) sorption properties (Fenta and Ali 2024; Tetteh *et al.* 2024).

Table 1. Codes and Levels of Experimental Factors for BBD

Experimental Variable	Symbol	Units	Coded Levels and Values		
			-1	0	+1
Wheat straw size	A	mm	0.1	0.3	0.5
Modifier concentration	B	mol/L	1	2	3
Term pyrolysis temperature	C	℃	300	500	700

Adsorption Kinetics Experiments of The Biochar for Cr(VI)

The kinetic studies employed adsorption data gathered by examining temperature and time effects. The adsorption kinetics of target biochars for Cr(VI) were determined by adding 0.1 g of the optimized WBC to 50 mL of a 50 mg/L Cr(VI) solution. The adsorption experiments were conducted at 25, 35, and 45 °C under continuous agitation at 150 r/min. Supernatant samples were taken at 10, 30, 60, 120, 240, 480, 720, 960, and 1440 min to measure the concentration of Cr(VI).

The rate kinetics for Cr(VI) uptake was examined by both pseudo-first-order (Eq. 3) and pseudo-second-order (Eq. 4) models (Tran *et al.* 2017; Wang *et al.* 2020). The standard equation for both models is described below.

The pseudo-first-order kinetics is given by Eq. 3,

$$ln(q_e - q_t) = ln\,(q_e - k_1 t) \quad (3)$$

where q_t and q_e (mg/g) denote the adsorption uptake of Cr(Vl) at any time t (min) and at equilibrium, and k_1 denotes the first order rate constant (min^{-1}).

Similarly, pseudo-second-order rate equation is given by Eq. 4,

$$\frac{t}{q_t} = \frac{1}{(k_2 \cdot q_e^2)} + \frac{t}{q_e} \quad (4)$$

where k_2 (g/mg min) represents rate constant for second order.

Adsorption Isotherm Experiments of the MWSB for Cr(VI)

Adsorption isotherm experiments for target heavy metal ions were performed by adding 0.1 g of MWSB to 50 mL Cr(VI) solutions with concentrations ranging from 10 to 250 mg/L (10, 25, 50, 100, 150, 200, 250 mg/L) under varying temperatures (25, 35, 45 ℃), pH 2, and a rotational speed of 150 r/min. The residual Cr(VI) concentration in each solution was determined following a 24-h reaction period. Langmuir (Eq. 5) and Freundlich (Eq. 6) models were chosen to reveal adsorption mechanism and the adsorption performance of the adsorbent on Cr(VI) (Zhou *et al.* 2022). Their equations are shown as follows,

Langmuir model:

$$Q_e = \frac{Q_m \cdot K_L \cdot C_e}{1 + K_L \cdot C_e} \quad (5)$$

Freundlich model:

$$Q_e = K_F \cdot C_e^{1/n} \quad (6)$$

where C_e represents the adsorbent concentration (mg/L), Q_e denotes the equilibrium adsorption capacity (mg/g), Q_m is the maximum adsorption capacity (mg/g), and K_L stands for the adsorption equilibrium constant. K_F and n are Freundlich parameters, which are associated with the adsorbent type and adsorption temperature.

Characterization Method

The surface morphology and elemental composition of biochar were examined using scanning electron microscopy with energy dispersive X-ray spectroscopy (SEM-EDS, Quanta 250). A Raman spectrometer (Raman, inVia Reflex) was used to detect the structure characteristics of the carbon layer of biochar to obtain molecular vibration information and analyze its crystal structure according to the characteristic peak of the material. Thermo Fisher Nicolet 6700 FTIR was employed for an in-depth analysis of the molecular structure and chemical composition of the biochar. X-ray photoelectron spectroscopy (XPS, Thermo Kalpha) was employed to analyze the chemical composition and structural morphology of carbon materials.

RESULTS AND DISCUSSION

Response Surface Design and Results

According to the BBD experimental design, with wheat straw size (WSS), modifier concentration (MC), and term pyrolysis temperature (CT) as the influencing factors and Cr(VI) removal efficiency as the response value, the Cr(VI) adsorption performance of wheat straw biochar was optimized. The experimental design and results are shown in Table 2.

Table 2. BBD Design and Experimental Results

Run	Factor 1	Factor 2	Factor 3	Response
	A:WWS (mm)	B:MC (mol/L)	C:CT (℃)	Removal efficiency of Cr(VI) (%)
1	1	0	1	48.22
2	1	0	-1	52.25
3	0	0	0	73.65
4	1	-1	0	55.23
5	1	1	0	65.53
6	0	0	0	71.66
7	0	-1	1	53.59
8	0	1	1	61.17
9	-1	1	0	89.45
10	0	0	0	70.29
11	-1	0	1	68.95
12	0	0	0	72.77
13	0	-1	-1	48.21
14	0	0	0	70.16
15	-1	0	-1	65.98
16	-1	-1	0	70.32
17	0	1	-1	65.84

The response model was developed by fitting experimental data using a quadratic multiple regression. Response surface methodology (RSM) was applied to establish the relationship between Cr(VI) removal efficiency and preparation parameters (A,B,C), as well as to analyze interactions among these parameters and their impact on removal performance. The response model (Eq. 7) incorporates positive sign (+) and the negative

sign (−) coefficients to represent synergistic and antagonistic effects, respectively, among the variables (Siddiqui *et al.* 2019).

$$Removal\ efficiency\ of\ Cr(VI) = 71.706 - 9.184 \times A + 6.83 \times B - 0.044 \times C - 2.208 \times AB - 1.75 \times AC - 2.513 \times BC + 0.037 \times A^2 - 1.611 \times B^2 - 12.893 \times C^2 \quad (7)$$

The variance analysis of the model is shown in Table 3.

Table 3. ANOVA for Quadratic Model

Source	Sum of Squares	df	Mean Square	F-value	p-value
Model	1829.47	9	203.27	98.04	< 0.0001
A-Wheat Straw Size	674.73	1	674.73	325.42	< 0.0001
B-Modifier concentration	373.19	1	373.19	179.99	< 0.0001
C-Term pyrolysis temperature	0.0153	1	0.0153	0.0074	0.9339
AB	19.49	1	19.49	9.4	0.0182
AC	12.25	1	12.25	5.91	0.0454
BC	25.25	1	25.25	12.18	0.0101
A^2	0.0058	1	0.0058	0.0028	0.9594
B^2	10.92	1	10.92	5.27	0.0554
C^2	699.91	1	699.91	337.56	< 0.0001
Residual	14.51	7	2.07		
Lack of Fit	5.21	3	1.74	0.7456	0.5786
Pure Error	9.31	4	2.33		
Cor Total	1843.98	16			

The Model F-value of 98.04 indicates the significance of the model, suggesting that the observed results are unlikely to be due to random variability. Model terms with p-values less than 0.05, such as A, B, AB, AC, BC, and C^2, are considered statistically significant. The Lack of Fit F-value, being 0.75, suggests that the Lack of Fit is not statistically significant, which is favorable for the model's adequacy (Kang *et al.* 2022).

Table 4. Statistical Analysis of Error of Regression Equation

Statistical Item	Numeric Value	Statistical Item	Numeric Value
Std. Dev.	1.44	R^2	0.9921
Mean	64.9	Adjusted R^2	0.982
C.V. %	2.22	Predicted R^2	0.9469
		Adeq Precision	36.6551

It can be seen from Table 4 that the fitted equation conformed to the above test principles and had good adaptability. The Predicted R^2, calculated as 0.9469, is reasonably consistent with the adjusted R^2 of 0.9820, with a difference of less than 0.2. This suggests a good fit of the model to the data. The C.V. was less than 10%, indicating high reliability and accuracy of the experiment. Adeq Precision was within a reasonable range (a signal-to-noise ratio greater than 4 is considered reasonable) (Kang *et al.* 2022).

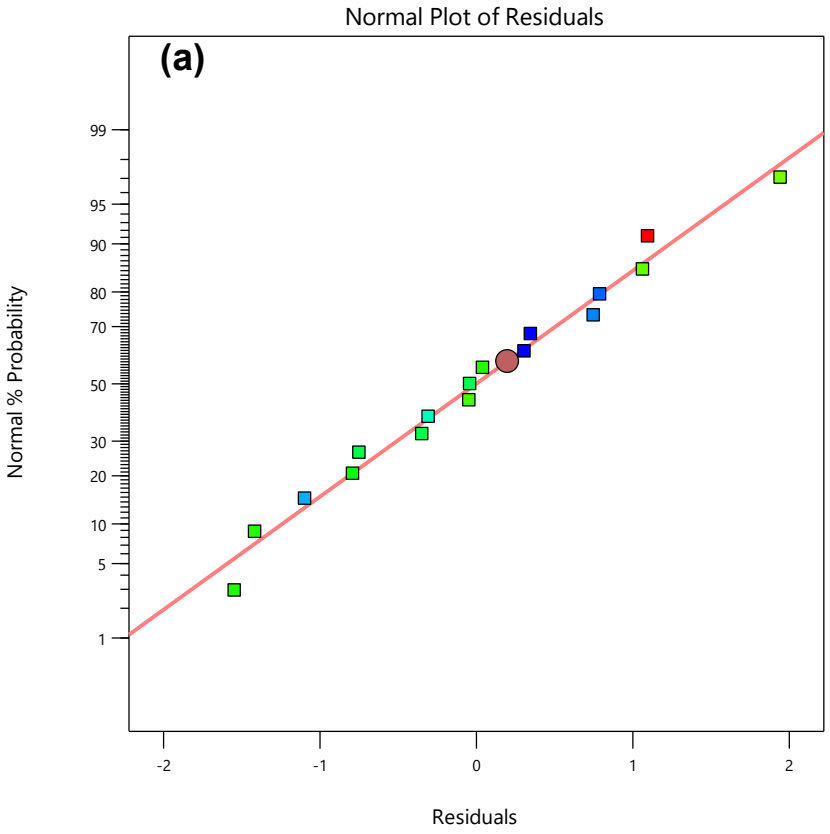
Normal Plot of Residuals
(a)
Normal % Probability
99
95
90
80
70
50
30
20
10
5
1
-2
-1
0
1
2
Residuals

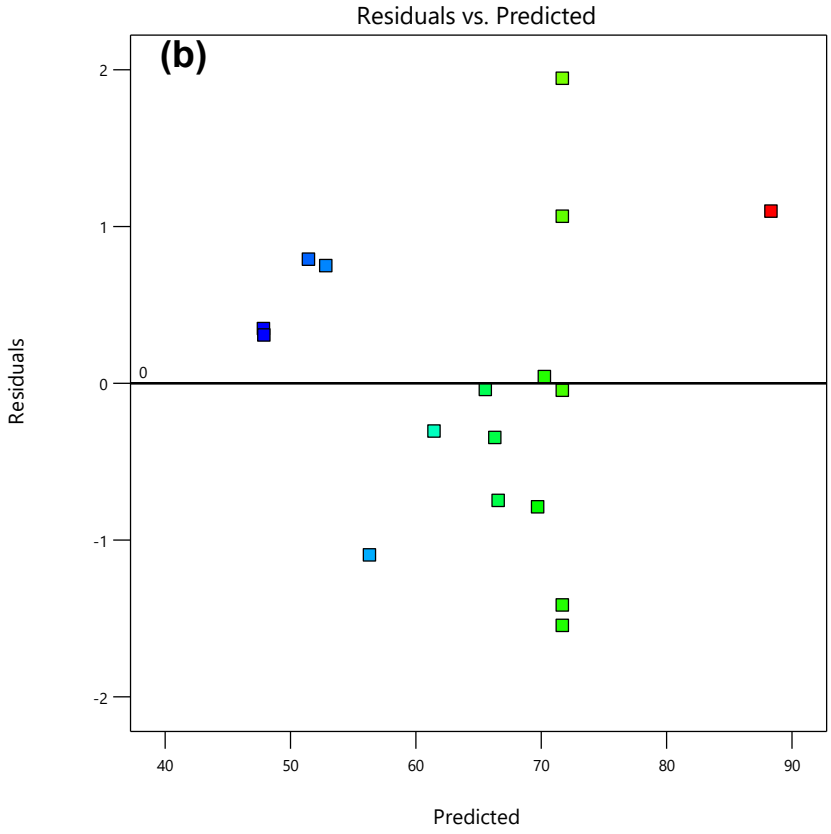
Residuals vs. Predicted
(b)
Residuals
2
1
0
-1
-2
40
50
60
70
80
90
Predicted

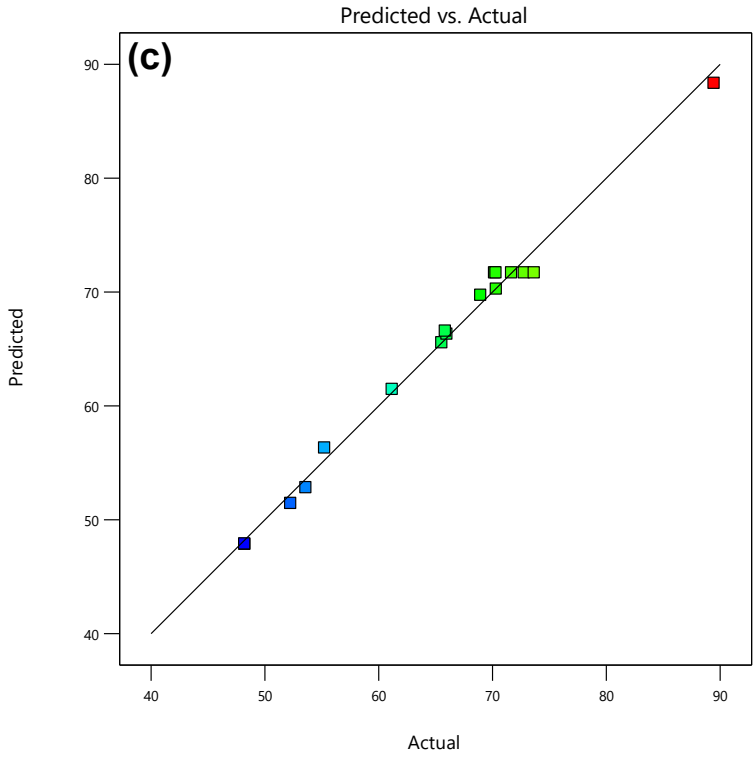

Fig. 1. (a) Normal probability distribution of residuals; (b) Distribution of residual and predicted values; (c) Distribution diagram of predicted and actual values

The normal probability distribution of the residuals is depicted in Fig. 1(a), illustrating a linear trend and suggesting an approximate normal distribution. Examining Fig. 1(b), it is evident that residuals and predicted values exhibited an irregular distribution, with residuals evenly dispersed on both sides of the horizontal line and no apparent skew. Despite the relatively large dispersion of residuals, this indicates that the model fitting the data lacked significant problems. Figure 1(c) reveals that the predicted values align well with the actual values, portraying an ideal scenario and affirming the model's robust predictive performance. The comprehensive analysis of these three figures establishes the model's strong adaptability and high reliability in predicting outcomes (Zhou *et al.* 2020).

Response Surface and Interaction Analysis

It can be observed from Fig. 2 that the contour lines in subfigures (a), (b), and (c) exhibited an elliptical pattern, indicating a significant pairwise interaction among the corresponding factors.

In Fig. 2(a), the relationship between wheat straw size and modifier concentration was found to be antagonistic. Specifically, at a wheat straw size of 0.1 mm, the removal efficiency increased from 70.3% to 89.5% with an increase in modifier concentration to 3 mol/L. Conversely, when the modifier concentration was 3 mol/L, the removal efficiency decreased to 65.5% with an increase in wheat straw size to 0.5 mm. Research by Ahmad and Danish (2018) shows that the smaller the particle size of straw raw material, the larger its specific surface area, which means that biochar has more adsorption sites, thus improving its ability to adsorb target substances (Ahmad and Danish 2018). Ding *et al.* (2023) believed that KOH acted as an activator in the pyrolysis process and could promote the etching of carbon in the straw powder, thus helping to improve the adsorption capacity

of biochar. To achieve the maximum removal efficiency, it is imperative to employ a relatively small wheat straw size coupled with a higher modifier concentration.

Analyzing Fig. 2(b), it is evident that the impact of wheat straw size and term pyrolysis temperature on each other was notably distinct. When the wheat straw size was 0.1 mm, the removal efficiency initially increased and then decreased with the rise in pyrolysis temperature, reaching its peak near 500 °C. At a pyrolysis temperature of 500 °C, the removal efficiency decreased further with an increase in wheat straw size. Iamsaard *et al.* (2023) showed that at medium and low temperatures (< 500 °C), straw biochar predominantly generates acidic oxygen-containing functional groups (*e.g.*, aliphatic functional group -COOH). As the temperature increased, the alkaline functional group (*e.g.*, aromatic functional group -COO-) on the biochar's surface became more dominant (Tripathi *et al.* 2016). Therefore, biochar prepared through low-temperature pyrolysis was more conducive to Cr(VI) removal. In conclusion, achieving a higher Cr(VI) removal efficiency involved preparing biochar under conditions of a smaller wheat straw size and a moderate term pyrolysis temperature.

Examining Fig. 2(c), it is evident that under the same term pyrolysis temperature, the Cr(VI) removal efficiency increased with an increase in KOH modifier concentration. Conversely, under the same modifier concentration, the removal efficiency initially increased and then decreased with increasing pyrolysis temperature, peaking near 500 °C. Wang *et al*. investigated the effects of pyrolysis temperature and KOH modifier concentration on the specific surface area and porosity of biochar. They found that aliphatic carboxylic groups and alkyl groups began to decompose with increasing pyrolysis temperature. Furthermore, KOH could remove impurities in biochar, optimize its pore structure, and improve its adsorption performance. Additionally, high pyrolysis temperature may also lead to partial pore structure collapse or excessive sintering of biochar, thus affecting its adsorption performance (Wang *et al.* 2020b). Consequently, biochar prepared under conditions of higher modifier concentration, and a moderate pyrolysis temperature yields a higher Cr(VI) removal efficiency.

(a)

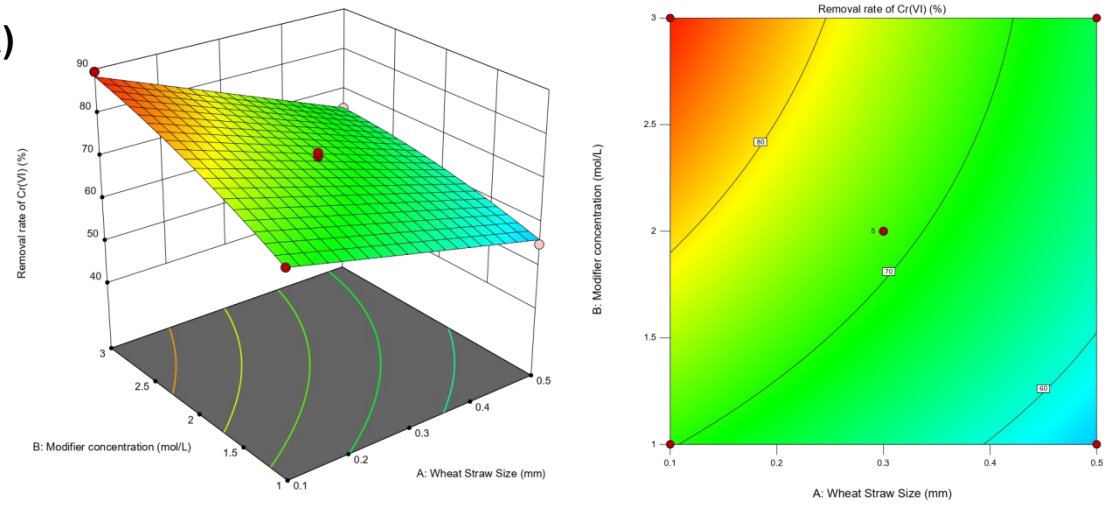

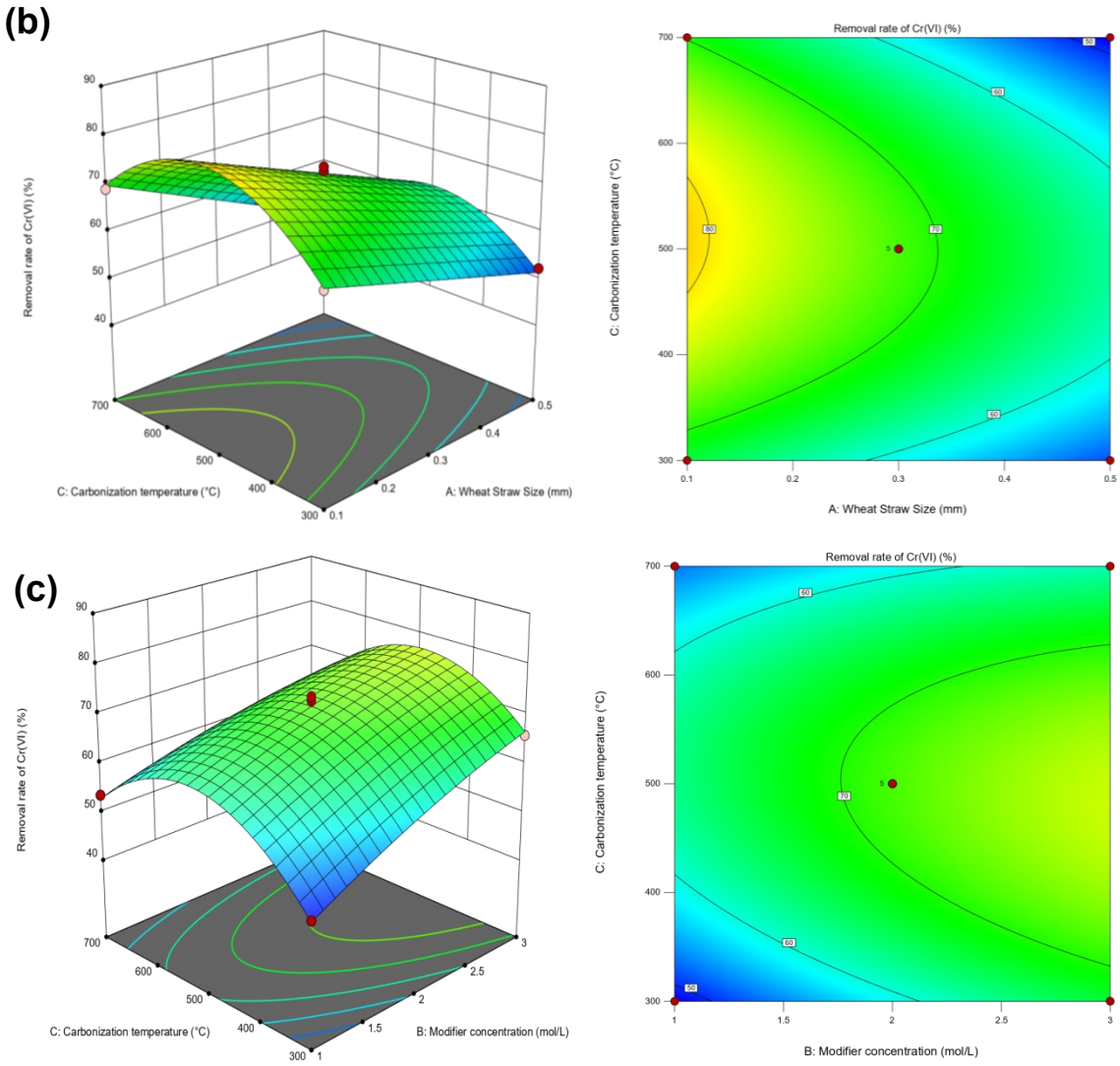

Fig. 2. The different factors that interact with the response surface

Considering the diverse factors interacting with the response surface in Fig. 2, it can be concluded that the straw size was inversely related to the removal efficiency, the modifier concentration was directly proportional to the removal efficiency, and the removal efficiency exhibited a trend of first increasing and then decreasing with the rise in term pyrolysis temperature. Therefore, to produce biochar with a superior Cr(VI) removal efficiency, it is advisable to adopt a smaller wheat straw size, a higher modifier concentration, and a moderate temperature. The smaller straw particle sizes provide greater specific surface area, thereby increasing the adsorption sites of biochar. Higher KOH concentrations optimize pore structure and remove impurities by enhancing etching activation. Meanwhile, moderate pyrolysis temperatures enrich the biochar surface with acidic oxygen-containing functional groups (*e.g.*, -COOH). The synergistic effects of these three factors are expected to significantly enhance biochar's adsorption capacity for Cr(VI).

Optimization of Preparation Conditions and Verification of Results

Through the optimization analysis of the experimental results by Design-Expert 13.0 software, the optimal combination of preparation conditions of MWSB were obtained as follows: a wheat straw size of 0.1 mm, KOH modifier concentration of 3 mol/L, and a term pyrolysis temperature of 493.8 ℃. The corresponding theoretical removal efficiency of Cr(VI) predicted value is 88.4%. In three parallel experiments under these conditions, the observed result was 86.5%, The prediction accuracy was 97.85% when compared with the theoretical value, indicating a satisfactory model performance.

Cr(VI) Adsorption Kinetics of MWSB

The kinetics curves for Cr(VI) removal by MWSB is displayed in Fig. 3.

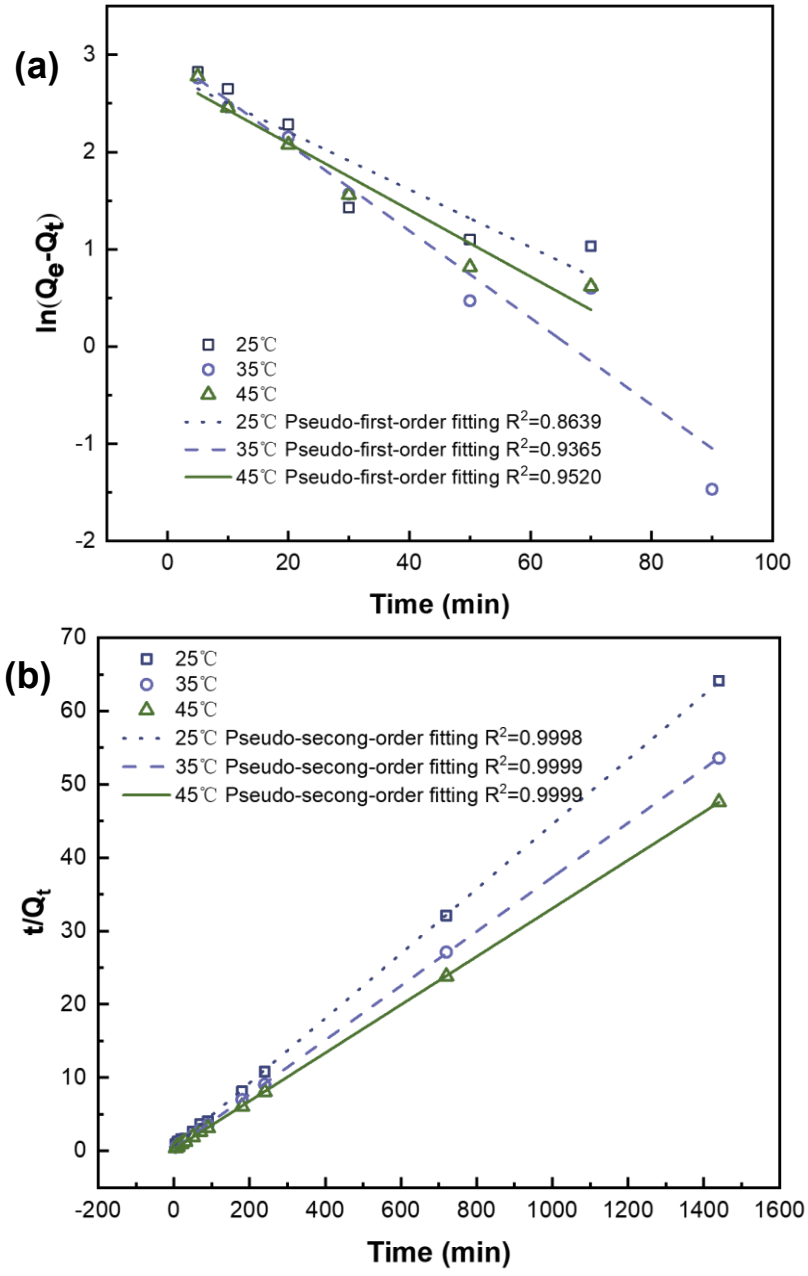

Fig. 3. Adsorption kinetics fitting curves of MWSB

Kinetic study for the adsorption process is essential, as it illustrates the adsorbate adsorption rate at solid-liquid interface depending on different reactions at the surface. The adsorption mechanism is highly dependent on the physicochemical characteristics of biochar, including mass transfer phenomena, as it is a complex process (Xie *et al.* 2021).

Graphical representation for both the kinetic models is displayed in Fig. 3(a) and (b), and the kinetic parameters are represented in Table 5. The high coefficients of determination (R^2), indicated that the experimental results fitted better with pseudo-second-order equation relative to pseudo-first-order kinetics.

Table 5. Kinetic Parameters for the Adsorption

T	PFO			PSO		
	K_1	Q_e	R^2	K_2	Q_e	R^2
25 °C	0.04499	22.0596	0.8639	0.0042	22.6706	0.9998
35 °C	0.06595	25.5806	0.9365	0.0043	27.0124	0.9999
45 °C	0.07924	28.6470	0.9520	0.0045	30.4414	0.9999

The pseudo-second-order kinetic model demonstrated clear linearity in the fitting results, as indicated by a coefficient of determination (R^2) of 0.99, where the fitted Q_e value closely matched the experimental value.

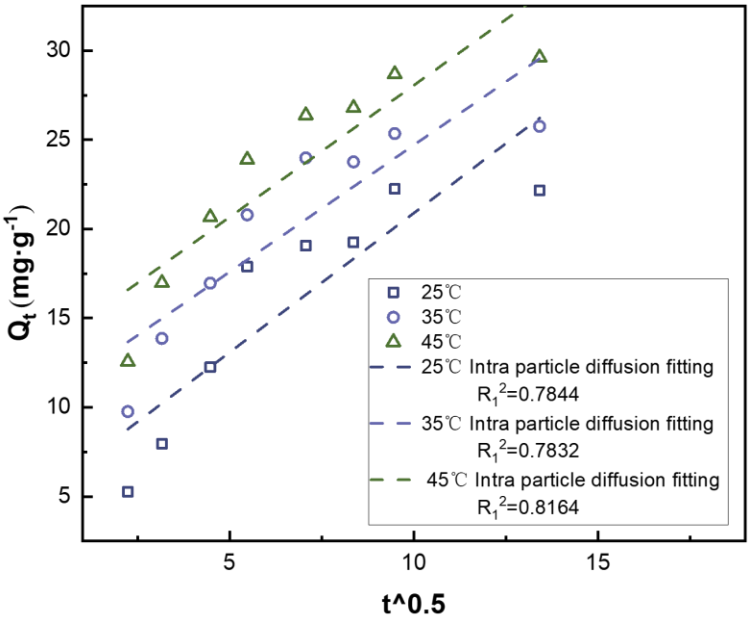

Fig. 4. Intra-particle diffusion kinetics fitting curves of MWSB

The adsorption process of adsorbents typically involves both film diffusion and intra-particle diffusion (Tran *et al.* 2017). Therefore, to elucidate the adsorption mechanism in greater detail, the intra-particle diffusion model was employed for a comprehensive analysis of the kinetic experimental data, followed by fitting procedures. As shown in Fig. 4, the model exhibited linear behavior during Cr(VI) adsorption, indicating that the removal process underwent a rapid phase governed by film diffusion before transitioning to an internal diffusion stage, with adsorption equilibrium reached around 4 h. The fitted curves did not pass through the origin, indicating that internal diffusion was not the sole rate-limiting step in the adsorption process (Guowen *et al.* 2026; Wang, B. *et al.* 2026).

Concurrently, the coefficient of determination R^2 suggested that the entire process conformed more closely to pseudo-second-order kinetics.

Cr(VI) Adsorption Equilibrium Isotherms of MWSB

To further study the adsorption capacity and mechanism of MWSB to Cr(VI) in water, a common isothermal adsorption model was used to carry out nonlinear fitting analysis on the experimental data, and the results are shown in Fig. 5 and Table 6.

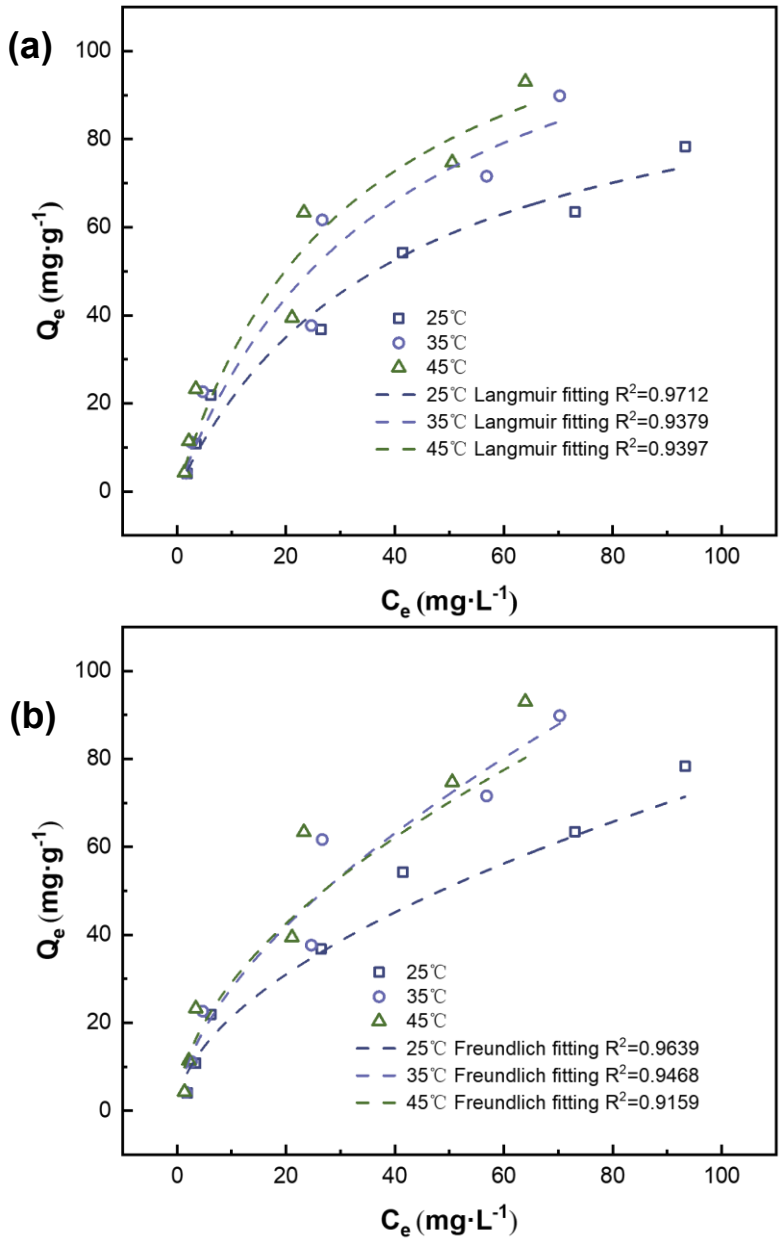

Fig. 5. Adsorption isotherm fitting curves of MWSB

As illustrated in Fig. 5 and summarized in Table 6, at temperatures of 25 and 45 °C, the Langmuir equation exhibited superior data fitting for Cr(VI) adsorption, yielding a higher coefficient of determination. Thus, the Langmuir equation proved to be a more

effective model for describing the adsorption behavior of Cr(VI) by MWSB in the solution. At temperatures of 25°C, the R^2 attained a high value of 0.9712, corresponding to a maximum adsorption capacity of 105 mg/g. The Langmuir isothermal adsorption model assumes adsorption occurs exclusively through active sites on the adsorbent's surface, specifically designed for homogeneous monolayer adsorption processes (Khalil *et al.* 2020). The absence of interactions between solute molecules during the adsorption process leans towards monolayer adsorption (Ali *et al.* 2020). At temperatures of 35 °C, the Freundlich equation adequately describes the adsorption process of Cr(VI) onto MWSB in solution, indicating that multi-layer adsorption occurs on the heterogeneous surface. The increase in temperature might have altered the distribution of chromium oxidation states, potentially promoting the reduction of Cr(VI) to Cr(III), thereby influencing the adsorption behaviour. This could explain the observed discrepancies in the adsorption isotherm model fitting at 35 °C.

Table 6. Parameters of Kinetic Models of MWSB

T	Langmuir			Freundlich		
	Q_m	K_1	R^2	*n*	K_F	R^2
25 ℃	105	0.0249	0.9712	1.84	6.10	0.9639
35 ℃	122	0.0250	0.9379	1.69	7.13	0.9468
45 ℃	132	0.0309	0.9397	1.83	8.30	0.9159

In the Freundlich model, the constants K_F and *n* depict the relationship between adsorption capacity and strength, with *n* also serving as the non-ideal index for the adsorbent surface. When $n > 1$, adsorption is favored, and when $n = 1$, it represents linear adsorption. Conversely, when $n < 1$, adsorption becomes nearly impossible. Notably, the calculated value of *n* in this study significantly exceeded 1, signifying the overall adsorption process is highly favorable (Trivedi *et al.* 2019; Zhou *et al.* 2022).

Characterization of the Samples

SEM and EDS

To comprehensively assess the impact of the modification process on the morphological characteristics of wheat straw biochar, SEM and EDS analyses were conducted on three distinct biochar materials: WSB, MWSB, and MWSB-Cr. The findings are illustrated in Fig. 6.

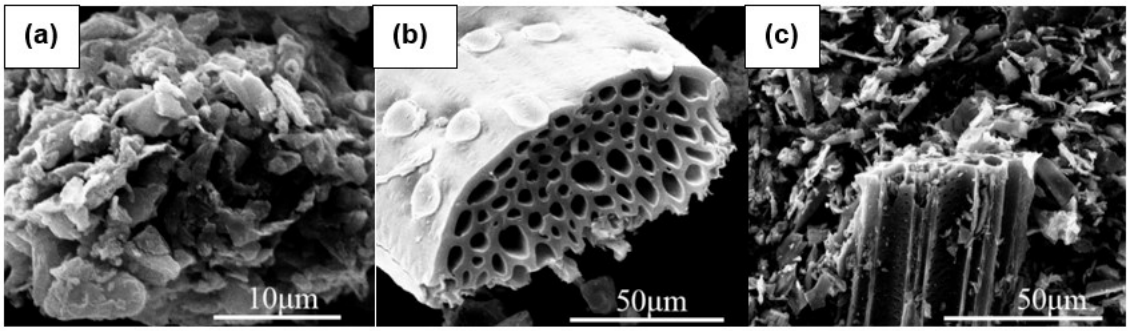

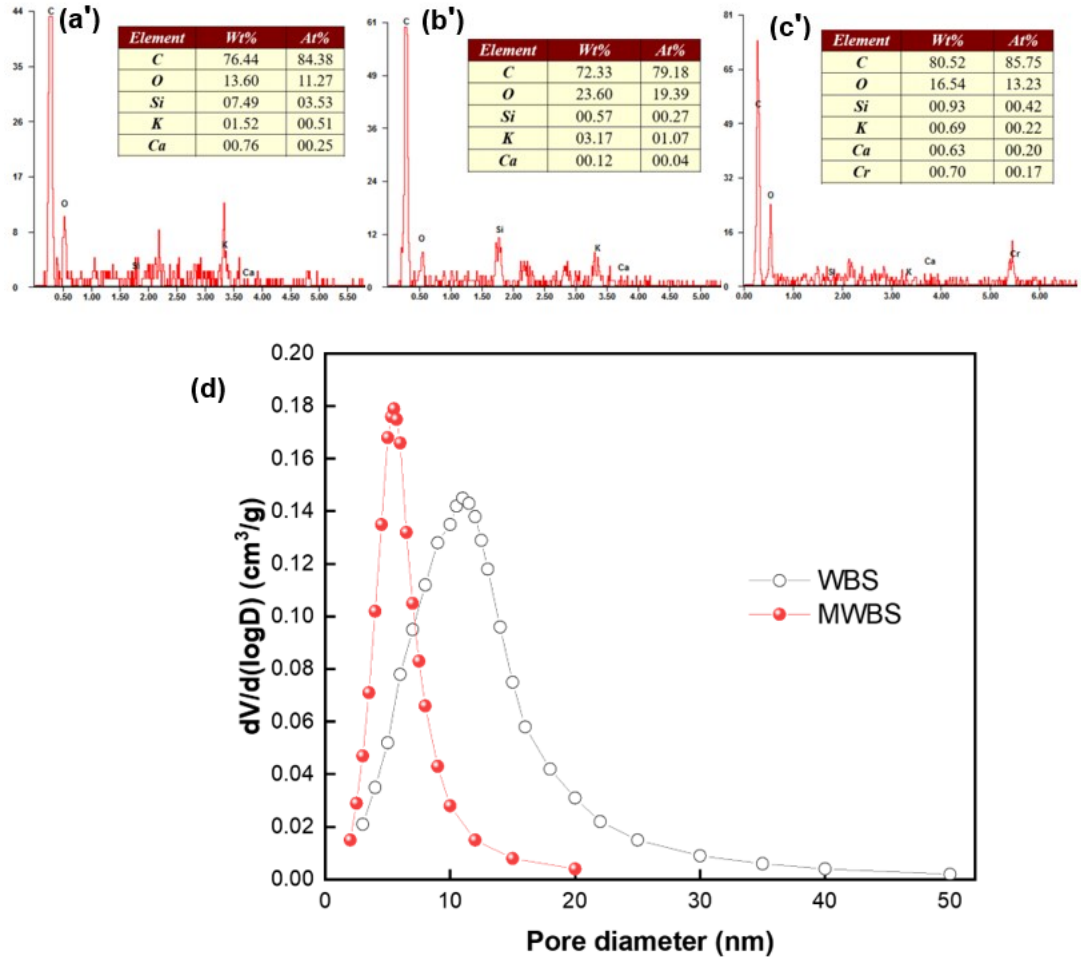

Fig. 6. SEM of WSB (a), MWSB (b) and MWSB-Cr (c); EDS of WSB (a'), MWSB (b') and MWSB-Cr (c') ; pore diameter distribution plots of WSB and MWSB (d)

As depicted in Fig. 6, prior to the modification process, the surface of the biochar particles appeared to be rough, exhibiting small cracks or bumps, yet lacking an evident pore structure (Fig. 6(a)). Following KOH modification, the biochar particles assumed a clear and uniform appearance, showcasing a smooth surface with a well-defined pore structure. This resulted in the formation of larger pores and cracks, thereby establishing a more intricate pore network (Fig. 6(b)).

The pore diameter distribution of WBS and MWBS was determined by BET analysis (Fig. 6(d)). MWBS material predominantly exhibited small mesopores with increased micropores. Compared to WBS (S_{BET} = 89 m²/g, V_t = 0.24 cm³/g), MWBS exhibited a larger specific surface area (S_{BET} = 165 m²/g) and total pore volume (V_t = 0.63 cm³/g). This indicates that MWBS provided a greater interaction area and more adsorption sites for Cr(VI) adsorption. This transformation may be attributed to the strong alkaline nature of KOH and its robust reaction at elevated temperatures, enhancing the pore-forming capability of wheat straw biochar and rendering it more conducive to the adsorption of hexavalent chromium in water (Wang *et al.* 2020b; Ding *et al.* 2023).

The EDS analysis served to further corroborate both the occurrence of the modification process and the effectiveness of the adsorption process. Following KOH modification, there was an increase in the surface oxygen content of the material (Fig. 6

(a') and (c')). Additionally, KOH can react with SiO_2 to form K_2SiO_3 or K_4SiO_4 (Abbaci *et al.* 2022; Huang *et al.* 2017). The reduced silicon content on the surface of MWSB materials indicates that KOH also participated in the removal of silica (Fig. 6(a') and(b')). The energy spectrum of the adsorbed material exhibited a pronounced peak corresponding to Cr, providing tangible evidence of the efficacy of the adsorption process (Zhou *et al.* 2020; Jamil *et al.* 2023).

Raman analysis

Raman spectral analysis typically exhibits D and G peaks around 1350 cm^{-1} and 1600 cm^{-1}, respectively, providing insights into the carbon structure of the material. Here, the D peak signifies the disorder and defect degree of the carbon material, the G peak represents the symmetry of the carbon material, and I_D/I_G reflects the degree of disorder (Siddiqui *et al.* 2019; Lu *et al.* 2022). Upon comparing the peak signals before and after KOH modification in Fig. 7, it becomes evident that the introduction of the modifier substantially increased the defects in the wheat straw biochar material. The I_D/I_G ratio also rose from 1.62 to 1.84, highlighting a more pronounced degree of disorder in the modified material. This undoubtedly facilitated the subsequent adsorption processes. Following the adsorption, significant alterations in the peak values of the adsorbent were observed, with the I_D/I_G decreasing to 0.86. This indicates that hexavalent chromium adhered to the surface of the material structure, filling the original surface irregularities to some extent (Tetteh *et al.* 2024).

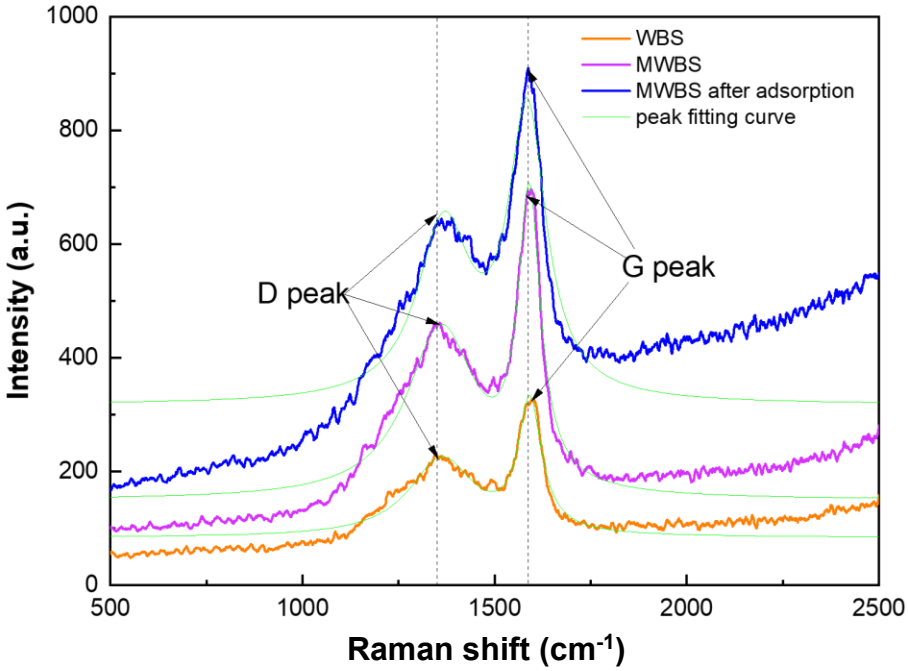

Fig. 7. Raman spectral analysis map of different materials

FTIR analysis

The infrared spectra of WSB, MWSB, and MWSB-Cr display absorption bands at 1091, 1639, and 3328-3526 cm^{-1}, corresponding to characteristic functional groups in biochar. Specifically, the broad band at 3328 to 3526 cm^{-1} is assigned to -OH and -NH- stretching vibrations (Li *et al.* 2019; Fenta and Ali 2024); the peak near 1639 cm^{-1}

correlates with C=O (ester) and O-H stretching vibrations (Siddiqui *et al.* 2019; Fenta and Ali 2024), and the 1091 cm^{-1} band indicates C-O vibrational absorption (Li *et al.* 2019).

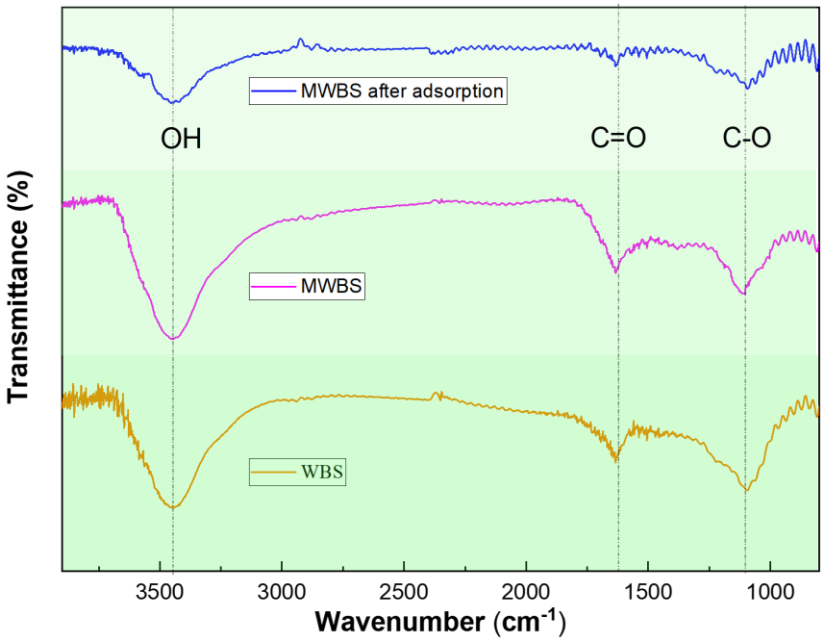

Fig. 8. FTIR analysis of different materials

Upon comparing the spectra before and after modification, significant differences in the characteristic functional groups at 3440 and 1095 cm^{-1} were observed. After modification, the peak value of biochar decreased at 1095 cm^{-1} and it increased at 3440 cm^{-1}, indicating an increase in the -OH content and emphasizing the crucial role of KOH modification (Wang *et al.* 2020b). Following the adsorption reaction, the absorption strength of -OH reached its peak, underscoring the significant involvement of -OH in hexavalent chromium removal from water (Ding *et al.* 2023). These oxygen-containing functional groups also facilitate the adsorption of Cr(VI) ions in the solution, showcasing the rapid removal characteristics.

XPS analysis

The XPS analysis of MWSB before and after Cr(VI) adsorption was conducted to characterize surface elemental composition and chemical states, as illustrated in Fig. 9.

Figure 9(a) displays the overall spectra of MWSB before and after adsorption. It reveals the presence of three elements: C, O, and K. Notably, a Cr peak was observed after adsorption, confirming the successful adsorption of hexavalent chromium. Figure 9(b) shows the high-resolution scan XPS spectrum of the C1s of MWSB, where the four peaks at 293.61, 290.19, 285.72, and 284.8 eV correspond to C π-π*, O-C=O, C-O, and C-C/C-H, respectively (Sun *et al.* 2023). As shown in Fig. 9(d) and 9(e), the characteristic peaks of O1s experienced a shift of about 0.7 eV; this shift indicates that the oxygen-active group participates in the redox reaction between O and Cr. Figure 9(f) characterizes the Cr 2p of the MWSB material after adsorption, with photoelectron peaks of Cr 2p3/2 and Cr 2p1/2 appearing at 576.50 eV and 586.59 eV, respectively (Luo *et al.* 2023; Qian *et al.* 2023).

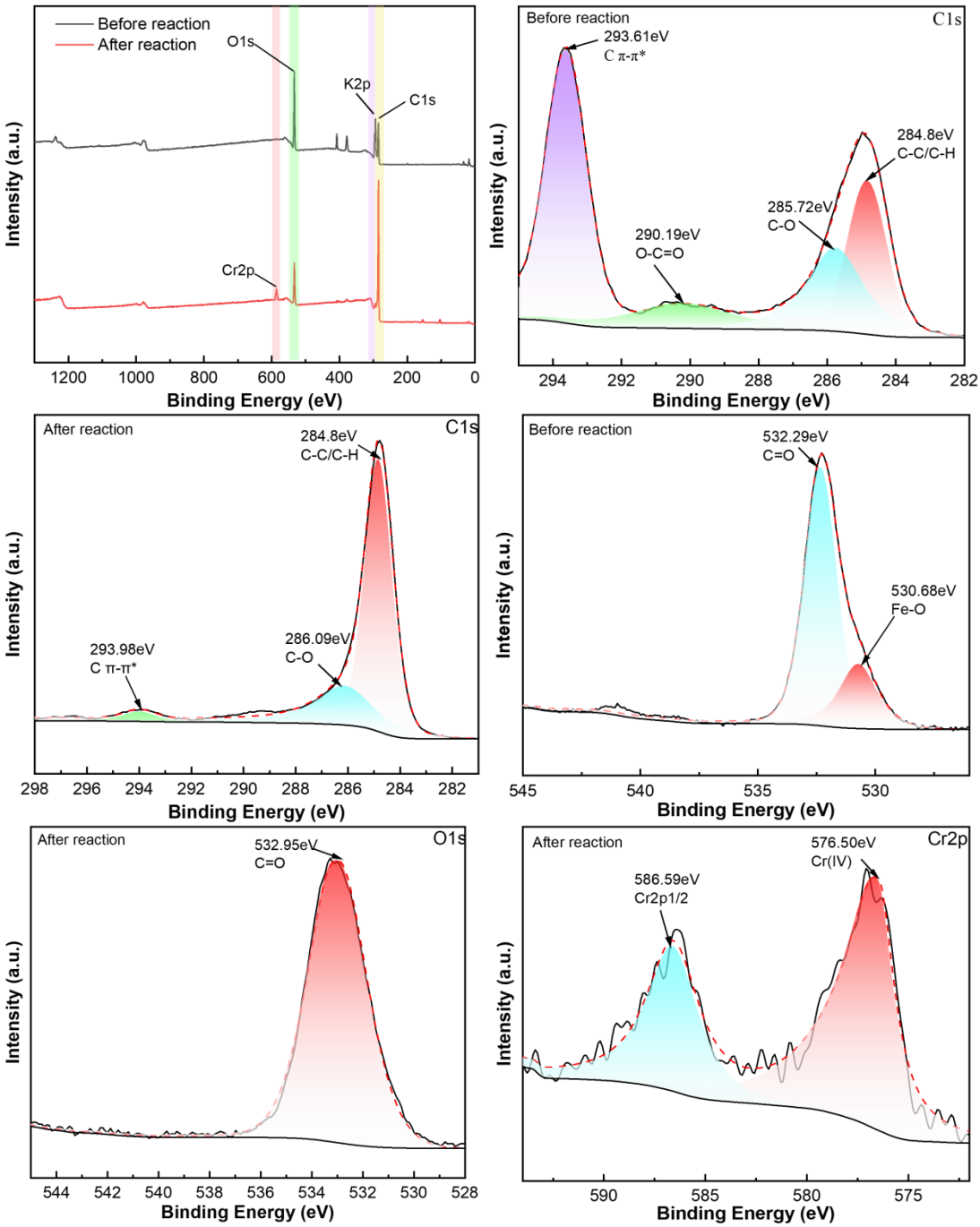

Fig. 9. (a) Wide-scan XPS spectra of MWSB and used MWSB, (b) C1s of MWSB, (c) C1s of used MWSB, (d) O1s of MWSB, (e) O1s of used MWSB, and (f) Cr 2p of used MWSB

Removal mechanisms of Cr(VI)

Based on the foregoing discussion, the Cr(VI) removal mechanism proposed is illustrated in Figure 10: (i) Adsorption: The abundant pore structure and oxygen-containing functional groups generated van der Waals forces between Cr(VI) and MWBS, enabling Cr(VI) removal through pore filling. (ii) Electrostatic attraction: Protonated oxygen-containing functional groups on the MWBS surface became positively charged, facilitating the adsorption of negatively charged Cr(VI) ions (*e.g.*, $HCrO_4^-$). (iii) Reduction: Surface

oxygen-containing groups on MWBS could act as electron donors, reducing some of the adsorbed hexavalent chromium to trivalent chromium (Shakya *et al.* 2022). (iv) Surface complexation: Cr(VI) (or Cr(III)) might also undergo surface complexation with MWBS surface functional groups through specific metal-ligand interactions (Ahmad *et al.* 2022).

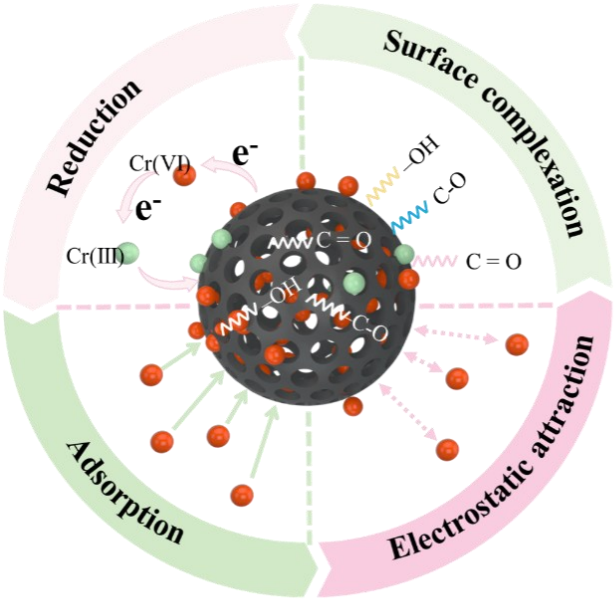

Fig. 10. Removal mechanisms of Cr(VI)

Future Perspectives

To advance the efficient synthesis of modified biochar and its application potential in wastewater treatment, future research must delve deeper into the following key areas:

1. Research into dynamic continuous-flow treatment processes for real wastewater: Overcoming the limitations of single/batch systems by transitioning to continuous-flow column adsorption processes, systematically evaluating their dynamic adsorption capacity, competitive selectivity, and practical engineering feasibility.
2. Data-driven optimisation through artificial intelligence and machine learning: Further leverage emerging tools such as machine learning (ML) and artificial intelligence (AI) to construct large-scale databases. Employ AI models to predict adsorption capacities and identify key influencing factors. Conduct in-depth analysis of micro-interaction mechanisms between adsorbents and pollutants under complex environmental conditions, providing deeper theoretical guidance for optimising synthesis pathways.

CONCLUSIONS

1. Adsorption Efficacy and Mechanism: Modified wheat straw biochar (MWSB) achieved an 86.5% Cr(VI) removal efficiency with a maximum adsorption capacity of 105 mg/g.
2. Adsorption Behavior: At temperatures of 25°C, isothermal adsorption aligned closely with the Langmuir model (R^2 = 0.9712), indicating monolayer adsorption. Kinetics were best described by the pseudo-second-order kinetic model.
3. Application Value: The preparation and application of this environmentally friendly adsorbent provide valuable theoretical insights for Cr(VI) removal from aqueous solutions.
4. Optimized Preparation: The RSM determined the optimal preparation parameters: wheat straw particle size of 0.1 mm, KOH modifier concentration of 3 mol/L, and pyrolysis temperature of 494 °C.

ACKNOWLEDGEMENTS

This research was funded by NSFC-China (No.42377490), Natural Science Foundation of Henan (No.232300421343), Project for Young Key Teachers of Henan Province (No.2020GGJS238), and the Doctoral Foundation of Henan University of Engineering (No. D2022016).

REFERENCES CITED

Abbaci, F., Nait-Merzoug, A., Guellati, O., Harat, A., El Haskouri, J., Delhalle, J., Mekhalif, Z., and Guerioune, M. (2022). "Bio/KOH ratio effect on activated biochar and their dye based wastewater depollution," *Journal of Analytical and Applied Pyrolysis* 162, article 105452. https://doi.org/10.1016/j.jaap.2022.105452

Ahmad, S., Gao, F., Lyu, H., Ma, J., Zhao, B., Xu, S., Ri, C., and Tang, J. (2022). "Temperature-dependent carbothermally reduced iron and nitrogen doped biochar composites for removal of hexavalent chromium and nitrobenzene," *Chemical Engineering Journal* 450, article 138006. https://doi.org/10.1016/j.cej.2022.138006

Ahmad, T., and Danish, M. (2018). "Prospects of banana waste utilization in wastewater treatment: A review," *Journal of Environmental Management* 206, 330-348. https://doi.org/10.1016/j.jenvman.2017.10.061

Ali, S., Noureen, S., Shakoor, M. B., Haroon, M. Y., Rizwan, M., Jilani, A., Arif, M. S., and Khalil, U. (2020). "Comparative evaluation of wheat straw and press mud biochars for Cr(VI) elimination from contaminated aqueous solution," *Environmental Technology & Innovation* 19, article 101017. https://doi.org/10.1016/j.eti.2020.101017

Altundogan, H. S. (2005). "Cr(VI) removal from aqueous solution by iron (III) hydroxide-loaded sugar beet pulp," *Process Biochemistry* 40(3–4), 1443-1452. https://doi.org/10.1016/j.procbio.2004.06.027

Ameen Hezam Saeed, A., Yub Harun, N., Mahmoud Nasef, M., Al-Fakih, A., Abdulhakim Saeed Ghaleb, A., and Kolawole Afolabi, H. (2022). "Removal of cadmium from aqueous solution by optimized rice husk biochar using response

surface methodology," *Ain Shams Engineering Journal* 13(1), article 101516. https://doi.org/10.1016/j.asej.2021.06.002

Ashfaq, A., Nadeem, R., Gong, H., Rashid, U., Noreen, S., Rehman, S. ur, Ahmed, Z., Adil, M., Akhtar, N., Ashfaq, M. Z., *et al.* (2022). "Fabrication of novel agrowaste (banana and potato peels)-based biochar/TiO_2 nanocomposite for adsorption of Cr(VI), statistical optimization via RSM approach," *Polymers* 14(13), article 2644. https://doi.org/10.3390/polym14132644

Bachmann, S. A. L., Dávila, I. V. J., Calvete, T., and Féris, L. A. (2022). "Adsorption of Cr(VI) on lignocellulosic wastes adsorbents: An overview and further perspective," *International Journal of Environmental Science and Technology* 19(12), 12727-12748. https://doi.org/10.1007/s13762-022-03928-z

Bian, H., Wang, M., Huang, J., Liang, R., Du, J., Fang, C., Shen, C., Man, Y. B., Wong, M. H., Shan, S., *et al.* (2024). "Large particle size boosting the engineering application potential of functional biochar in ammonia nitrogen and phosphorus removal from biogas slurry," *Journal of Water Process Engineering* 57, article 104640. https://doi.org/10.1016/j.jwpe.2023.104640

Bibi, I., Niazi, N. K., Choppala, G., and Burton, E. D. (2018). "Chromium(VI) removal by siderite ($FeCO_3$) in anoxic aqueous solutions: An X-ray absorption spectroscopy investigation," *Science of The Total Environment* 640–641, 1424-1431. https://doi.org/10.1016/j.scitotenv.2018.06.003

Chang, F., Yue, S., Li, S., Wang, H., Chen, Y., Yang, W., Wu, B., Sun, H., Wang, S., Yin, L., *et al*. (2025). "Periodic straw-derived biochar improves crop yield, sequesters carbon, and mitigates emissions," *European Journal of Agronomy* 164, article 127516. https://doi.org/10.1016/j.eja.2025.127516

Chen, D., Wang, X., Wang, X., Feng, K., Su, J., and Dong, J. (2020). "The mechanism of cadmium sorption by sulphur-modified wheat straw biochar and its application cadmium-contaminated soil," *Science of The Total Environment* 714, article 136550. https://doi.org/10.1016/j.scitotenv.2020.136550

Ćwieląg-Piasecka, I., Jamroz, E., Medyńska-Juraszek, A., Bednik, M., Kosyk, B., and Polláková, N. (2023). "Deashed wheat-straw biochar as a potential superabsorbent for pesticides," *Materials* 16(6), article 2185. https://doi.org/10.3390/ma16062185

Ding, E., Jiang, J., Lan, Y., Zhang, L., Gao, C., Jiang, K., Qi, X., and Fan, X. (2023). "Optimizing Cd^{2+} adsorption performance of KOH modified biochar adopting response surface methodology," *Journal of Analytical and Applied Pyrolysis* 169, article 105788. https://doi.org/10.1016/j.jaap.2022.105788

Fang, S., Huang, X., Xie, S., Du, J., Zhu, J., Wang, K., Zhuang, Q., and Huang, X. (2022). "Removal of chromium (VI) by a magnetic nanoscale zerovalent iron–assisted chicken manure-derived biochar: Adsorption behavior and synergetic mechanism," *Frontiers in Bioengineering and Biotechnology* 10, article 935525. https://doi.org/10.3389/fbioe.2022.935525

Fenta, A. A., and Ali, A. N. (2024). "Development of biochar/HDPE composites and characterization of the effects of carbon loadings on the electromagnetic shielding properties," *Heliyon* 10(2), article ID e24424. https://doi.org/10.1016/j.heliyon.2024.e24424

Govindaraju, K., Vinu, R., Gautam, R., Vasantharaja, R., Niranjan, M., and Sundar, I. (2024). "Microwave-assisted torrefaction of biomass Kappaphycus alvarezii–based biochar and magnetic biochar for removal of hexavalent chromium [Cr(VI)] from

aqueous solution," *Biomass Conversion and Biorefinery* 14(3), 3643-3653. https://doi.org/10.1007/s13399-022-02512-2

Huang, H., Tang, J., Gao, K., He, R., Zhao, H., Werner, D., (2017). "Characterization of KOH modified biochars from different pyrolysis temperatures and enhanced adsorption of antibiotics," *RSC Adv*. 7, article 14640-14648. https://doi.org/10.1039/C6RA27881G

Iamsaard, K., Weng, C.-H., Tzeng, J.-H., Anotai, J., Jacobson, A. R., and Lin, Y.-T. (2023). "Systematic optimization of biochars derived from corn wastes, pineapple leaf, and sugarcane bagasse for Cu(II) adsorption through response surface methodology," *Bioresource Technology* 382, article 129131. https://doi.org/10.1016/j.biortech.2023.129131

Irfan, M., Ishaq, F., Muhammad, D., Khan, M. J., Mian, I. A., Dawar, K. M., Muhammad, A., Ahmad, M., Anwar, S., Ali, S., *et al.* (2021). "Effect of wheat straw derived biochar on the bioavailability of Pb, Cd and Cr using maize as test crop," *Journal of Saudi Chemical Society* 25(5), article 101232. https://doi.org/10.1016/j.jscs.2021.101232

Islam, Md. A., Angove, M. J., and Morton, D. W. (2019). "Recent innovative research on chromium (VI) adsorption mechanism," *Environmental Nanotechnology, Monitoring & Management* 12, article 100267. https://doi.org/10.1016/j.enmm.2019.100267

Jain, S. (2026). "Optimized in-situ transesterification of spirogyra using KOH-activated wheat straw biochar catalyst," *Results in Engineering* 29, article 108896. https://doi.org/10.1016/j.rineng.2025.108896

Jamil, U., Zeeshan, M., Khan, S. R., and Saeed, S. (2023). "Synthesis and two-step KOH based activation of porous biochar of wheat straw and waste tire for adsorptive exclusion of chromium (VI) from aqueous solution; thermodynamic and regeneration study," *Journal of Water Process Engineering* 53, article 103892. https://doi.org/10.1016/j.jwpe.2023.103892

Junjie, L., Xiaobin, Y., Meiyi, Z., Tianshu, L., Zhimei, S., (2025). "Analysis of yield distribution and utilization of crop straw resources in China," *Journal of Agricultural Resources and Environment* 42(03), article 751-760. https://doi.org/10.13254/j.jare.2024.0184

Kang, J.-K., Seo, E.-J., Lee, C.-G., Jeong, S., and Park, S.-J. (2022). "Application of response surface methodology and artificial neural network for the preparation of Fe-loaded biochar for enhanced Cr(VI) adsorption and its physicochemical properties and Cr(VI) adsorption characteristics," *Environmental Science and Pollution Research* 29(40), 60852-60866. https://doi.org/10.1007/s11356-022-20009-3

Kapoor, R. T., Treichel, H., and Shah, M. P. (2021). *Biochar and Its Application in Bioremediation*, R. Thapar Kapoor, H. Treichel, and M. P. Shah (eds.), Springer Nature Singapore, Singapore. https://doi.org/10.1007/978-981-16-4059-9

Khalil, U., Bilal Shakoor, M., Ali, S., Rizwan, M., Nasser Alyemeni, M., and Wijaya, L. (2020). "Adsorption-reduction performance of tea waste and rice husk biochars for Cr(VI) elimination from wastewater," *Journal of Saudi Chemical Society* 24(11), 799-810. https://doi.org/10.1016/j.jscs.2020.07.001

Krasucka, P., Pan, B., Sik Ok, Y., Mohan, D., Sarkar, B., and Oleszczuk, P. (2021). "Engineered biochar – A sustainable solution for the removal of antibiotics from water," *Chemical Engineering Journal* 405, article 126926. https://doi.org/10.1016/j.cej.2020.126926

Lalmalsawmdawngliani, Lalhriatpuia, C., and Tiwari, D. (2024). "Biochar-derived nanocomposites for environmental remediation: The insights and future perspectives," *Journal of Environmental Chemical Engineering* 12(1), article 111840. https://doi.org/10.1016/j.jece.2023.111840

Li, J. H., Wang, P., Zhuang, K. Z., Bian, J. B., Tang, H. J., Guo, Y. P., and Song, J. Q. (2019). "Optimization, characterization, and Cr(VI) adsorption properties of iron oxide-coated wheat straw biochar," *Journal of Agro-Environment Science* 38(8), 1991-2001. https://doi.org/10.11654/jaes.2019-0004

Li, J.-h., Lv, G.-h., Bai, W.-b., Liu, Q., Zhang, Y.-c., Song, J.-q., (2016). "Modification and use of biochar from wheat straw (*Triticum aestivum* L.) for nitrate and phosphate removal from water," *Desalination and Water Treatment* 57(10), article 4681-4693. https://doi.org/10.1080/19443994.2014.994104

Lin, C., Luo, W., Luo, T., Zhou, Q., Li, H., and Jing, L. (2018). "A study on adsorption of Cr(VI) by modified rice straw: Characteristics, performances and mechanism," *Journal of Cleaner Production* 196, 626-634. https://doi.org/10.1016/j.jclepro.2018.05.279

Liu, C., Fiol, N., Villaescusa, I., and Poch, J. (2016). "New approach in modeling Cr(VI) sorption onto biomass from metal binary mixtures solutions," *Science of The Total Environment* 541, 101-108. https://doi.org/ 10.1016/j.scitotenv.2015.09.020

Liu, Y., Zhao, X., Li, J., Ma, D., Han, R., (2012). "Characterization of bio-char from pyrolysis of wheat straw and its evaluation on methylene blue adsorption," *Desalination and Water Treatment* 46(1), article 115-123. https://doi.org/10.1080/19443994.2012.677408

Liu, Z. T., Shao, J., Li, Y., Wu, Y. R., An, Y., Sun, Y. F., and Fei, Z. H. (2022). "Adsorption performance of tetracycline in water by alkali-modified wheat straw biochars," *Zhongguo Huanjing Kexue/China Environmental Science* 42(8), 3736-3743. https://doi.org/10.3969/j.issn.1000-6923.2022.08.031

Lu, T., Wang, X., Du, Z., and Wu, L. (2021). "Impacts of continuous biochar application on major carbon fractions in soil profile of North China Plain's cropland: In comparison with straw incorporation," *Agriculture, Ecosystems & Environment* 315, article 107445. https://doi.org/10.1016/j.agee.2021.107445

Lu, Y., Cai, Y., Zhang, S., Zhuang, L., Hu, B., Wang, S., Chen, J., and Wang, X. (2022). "Application of biochar-based photocatalysts for adsorption-(photo)degradation/ reduction of environmental contaminants: Mechanism, challenges and perspective," *Biochar* 4(1), article 45. https://doi.org/10.1007/s42773-022-00173-y

Luo, K., Lin, N., Li, X., Pang, Y., Wang, L., Lei, M., and Yang, Q. (2023). "Efficient hexavalent chromium removal by nano-cerium oxide functionalized biochar: Insight into the role of reduction," *Journal of Environmental Chemical Engineering* 11(3), article 110004. https://doi.org/10.1016/j.jece.2023.110004

Lyu, H., Tang, J., Huang, Y., Gai, L., Zeng, E. Y., Liber, K., and Gong, Y. (2017). "Removal of hexavalent chromium from aqueous solutions by a novel biochar supported nanoscale iron sulfide composite," *Chemical Engineering Journal* 322, 516-524. https://doi.org/10.1016/j.cej.2017.04.058

Ma, Y., Zhang, K., Li, D., Guo, M., Zhou, Y., Li, X., Miao, R., (2025). "Effects of wheat straw biochar with different proportions on phytoremediation efficiency and microbial communities of PAH-contaminated soils," *Journal of Environmental Chemical Engineering* 13(3), article 117140. https://doi.org/10.1016/j.jece.2025.117140

Nartey, O. D., and Zhao, B. (2014). "Biochar preparation, characterization, and adsorptive capacity and its effect on bioavailability of contaminants: An overview," *Advances in Materials Science and Engineering* 2014, article 715398. https://doi.org/10.1155/2014/715398

Peiris, C., Gunatilake, S. R., Mlsna, T. E., Mohan, D., and Vithanage, M. (2017). "Biochar based removal of antibiotic sulfonamides and tetracyclines in aquatic environments: A critical review," *Bioresource Technology* 246, 150-159. https://doi.org/10.1016/j.biortech.2017.07.150

Qian, L., Long, Y., Li, H., Wei, Z., Liang, C., Liu, R., and Chen, M. (2023). "Unveiling the role of biochar in simultaneous removal of hexavalent chromium and trichloroethylene by biochar supported nanoscale zero-valent iron," *Science of The Total Environment* 889, article 164243. https://doi.org/10.1016/j.scitotenv.2023.164243

Qiu, Y., Zhang, Q., Gao, B., Li, M., Fan, Z., Sang, W., Hao, H., and Wei, X. (2020). "Removal mechanisms of Cr(VI) and Cr(III) by biochar supported nanosized zero-valent iron: Synergy of adsorption, reduction and transformation," *Environmental Pollution* 265, article 115018. https://doi.org/10.1016/j.envpol.2020.115018

Saini, K., Biswas, B., Kumar, A., Sahoo, A., Kumar, J., and Bhaskar, T. (2022). "Screening of sugarcane bagasse-derived biochar for phenol adsorption: Optimization study using response surface methodology," *International Journal of Environmental Science and Technology* 19(9), 8797-8810. https://doi.org/10.1007/s13762-021-03637-z

Santhosh, C., Daneshvar, E., Tripathi, K. M., Baltrėnas, P., Kim, T., Baltrėnaitė, E., and Bhatnagar, A. (2020). "Synthesis and characterization of magnetic biochar adsorbents for the removal of Cr(VI) and Acid orange 7 dye from aqueous solution," *Environmental Science and Pollution Research* 27(26), 32874-32887. https://doi.org/10.1007/s11356-020-09275-1

Shakya, A., Vithanage, M., Agarwal, T. (2022). "Influence of pyrolysis temperature on biochar properties and Cr(VI) adsorption from water with groundnut shell biochars: Mechanistic approach," *Environmental Research* 215, article 114243. https://doi.org/10.1016/j.envres.2022.114243

Siddiqui, M. T. H., Nizamuddin, S., Mubarak, N. M., Shirin, K., Aijaz, M., Hussain, M., and Baloch, H. A. (2019). "Characterization and process optimization of biochar produced using novel biomass, waste pomegranate peel: A response surface methodology approach," *Waste and Biomass Valorization* 10(3), 521-532. https://doi.org/10.1007/s12649-017-0091-y

Sinha, R., Kumar, R., Abhishek, K., Shang, J., Bhattacharya, S., Sengupta, S., Kumar, N., Singh, R. K., Mallick, J., Kar, M., *et al.* (2022). "Single-step synthesis of activated magnetic biochar derived from rice husk for hexavalent chromium adsorption: Equilibrium mechanism, kinetics, and thermodynamics analysis," *Groundwater for Sustainable Development* 18, article 100796. https://doi.org/10.1016/j.gsd.2022.100796

Sun, Y., Lyu, H., Gai, L., Sun, P., Shen, B., and Tang, J. (2023). "Biochar-anchored low-cost natural iron-based composites for durable hexavalent chromium removal," *Chemical Engineering Journal* 476, article 146604. https://doi.org/10.1016/j.cej.2023.146604

Tetteh, I. K., Issahaku, I., and Tetteh, A. Y. (2024). "Recent advances in synthesis, characterization, and environmental applications of activated carbons and other

carbon derivatives," *Carbon Trends* 14, article 100328. https://doi.org/10.1016/j.cartre.2024.100328

Tran, H.N., You, S.-J., Hosseini-Bandegharaei, A., Chao, H.-P., (2017). "Mistakes and inconsistencies regarding adsorption of contaminants from aqueous solutions: A critical review," *Water Research* 120, article ID 88-116. https://doi.org/10.1016/j.watres.2017.04.014

Tripathi, M., Sahu, J. N., and Ganesan, P. (2016). "Effect of process parameters on production of biochar from biomass waste through pyrolysis: A review," *Renewable and Sustainable Energy Reviews* 55, 467-481. https://doi.org/10.1016/j.rser.2015.10.122

Trivedi, N. S., Kharkar, R. A., and Mandavgane, S. A. (2019). "Use of wheat straw combustion residues for removal of chlorinated herbicide (2,4-dichlorophenoxyacetic acid)," *Waste and Biomass Valorization* 10(5), 1323-1331. https://doi.org/10.1007/s12649-017-0134-4

Wang, J., and Wang, S. (2019). "Preparation, modification and environmental application of biochar: A review," *Journal of Cleaner Production* 227, 1002-1022. https://doi.org/10.1016/j.jclepro.2019.04.282

Wang, H., Xu, J., and Sheng, L. (2020a). "Preparation of straw biochar and application of constructed wetland in China: A review," *Journal of Cleaner Production* 273, article 123131. https://doi.org/10.1016/j.jclepro.2020.123131

Wang, L., Bolan, N. S., Tsang, D. C. W., and Hou, D. (2020b). "Green immobilization of toxic metals using alkaline enhanced rice husk biochar: Effects of pyrolysis temperature and KOH concentration," *Science of the Total Environment* 720, article 137584. https://doi.org/10.1016/j.scitotenv.2020.137584

Wang, J., and Guo, X., (2020). "Adsorption kinetic models: Physical meanings, applications, and solving methods," *Journal of Hazardous Materials* 390, article 122156. https://doi.org/10.1016/j.jhazmat.2020.122156

Wang, H., Xu, J., Liu, X., and Sheng, L. (2021). "Preparation of straw activated carbon and its application in wastewater treatment: A review," *Journal of Cleaner Production* 283, article 124671. https://doi.org/10.1016/j.jclepro.2020.124671

Wang, Q., Yue, Y., Liu, W., Liu, Q., Song, Y., Ge, C., and Ma, H. (2023). "Removal performance of KOH-modified biochar from tropical biomass on tetracycline and Cr(VI)," Materials 16(11), Article ID 3994. https://doi.org/10.3390/ma16113994

Wang, Z., Li, J., Kang, Y., Ran, J., Song, J., Jiang, M., Li, W., Zhang, M. (2025). "Effects of wheat straw-derived biochar on soil microbial communities under phenanthrene stress," *Agriculture* 15(1), article 15010077.

Wang, M., Luo, Y., Tuerhong, T., Wang, Y. (2026). "Adsorption of arsenic–fluorine in groundwater by Fe/La-modified wheat straw–derived biochar," *Materials Chemistry and Physics* 348, article 131606. https://doi.org/10.1016/j.matchemphys.2025.131606

Xiao, Y., Liu, L., Han, F., and Liu, X. (2022). "Mechanism on Cr(VI) removal from aqueous solution by camphor branch biochar," *Heliyon* 8(8), article e10328. https://doi.org/10.1016/j.heliyon.2022.e10328

Xie, J., Lin, R., Liang, Z., Zhao, Z., Yang, C., and Cui, F. (2021). "Effect of cations on the enhanced adsorption of cationic dye in Fe3O4-loaded biochar and mechanism," *Journal of Environmental Chemical Engineering* 9(4), article ID 105744. https://doi.org/10.1016/j.jece.2021.105744

Yan, Q., Tian, H., Huang, Y., Mu, X., Tang, G., Ma, H., Megharaj, M., Xu, W., He, W., (2025). "Recycled wheat straw biochar enhances nutrient-poor soil: Enzymatic

kinetics of carbon, nitrogen, and phosphorus cycling," *Journal of Environmental Management* 380, article 124950. https://doi.org/10.1016/j.jenvman.2025.124950

Yavari, S., Malakahmad, A., Sapari, N. B., and Yavari, S. (2017). "Sorption properties optimization of agricultural wastes-derived biochars using response surface methodology," *Process Safety and Environmental Protection* 109, 509-519. https://doi.org/10.1016/j.psep.2017.05.002

Yu, S., Zhang, W., Dong, X., Wang, F., Yang, W., Liu, C., and Chen, D. (2024). "A review on recent advances of biochar from agricultural and forestry wastes: Preparation, modification and applications in wastewater treatment," *Journal of Environmental Chemical Engineering* 12(1), article ID 111638. https://doi.org/10.1016/j.jece.2023.111638

Zeng, H., Zeng, H., Zhang, H., Shahab, A., Zhang, K., Lu, Y., Nabi, I., Naseem, F., and Ullah, H. (2021). "Efficient adsorption of Cr(VI) from aqueous environments by phosphoric acid activated eucalyptus biochar," *Journal of Cleaner Production* 286, article 124964. https://doi.org/10.1016/j.jclepro.2020.124964

Zhang, B., Zhou, S., Zhou, L., Wen, J., and Yuan, Y. (2019). "Pyrolysis temperature-dependent electron transfer capacities of dissolved organic matters derived from wheat straw biochar," *Science of The Total Environment* 696, article ID 133895. https://doi.org/10.1016/j.scitotenv.2019.133895

Zhang, R., Jing, J., Tao, J., Hsu, S.-C., Wang, G., Cao, J., Lee, C. S. L., Zhu, L., Chen, Z., Zhao, Y., *et al.* (2013). "Chemical characterization and source apportionment of PM 2.5 in Beijing: Seasonal perspective," *Atmospheric Chemistry and Physics* 13(14), 7053-7074. https://doi.org/10.5194/acp-13-7053-2013

Zhao, J., Li, Z., Wang, J., Li, Q., and Wang, X. (2015). "Capsular polypyrrole hollow nanofibers: An efficient recyclable adsorbent for hexavalent chromium removal," *Journal of Materials Chemistry A* 3(29), 15124-15132. https://doi.org/10.1039/C5TA02525G

Zhong, S., Hou, P., Zheng, C., Yang, X., Tao, Q., and Sun, J. (2025). "Wheat straw biochar amendment increases salinity stress tolerance in alfalfa seedlings by modulating physiological and biochemical responses," *Plants* 14(13), article 1954. https://doi.org/10.3390/plants14131954

Zhou, Q., and Sun, T. (2002). "Effects of chromium (VI) on extractability and plant uptake of fluorine in agricultural soils of Zhejiang Province, China," *Water, Air, and Soil Pollution* 133(1–4), 145-160. https://doi.org/10.1023/A:1012948131082

Zhou, R., Zhang, M., and Shao, S. (2022). "Optimization of target biochar for the adsorption of target heavy metal ion," *Scientific Reports* 12(1), article 13662. https://doi.org/10.1038/s41598-022-17901-w

Zhou, R., Zhang, M., Li, J., and Zhao, W. (2020). "Optimization of preparation conditions for biochar derived from water hyacinth by using response surface methodology (RSM) and its application in Pb^{2+} removal," *Journal of Environmental Chemical Engineering* 8(5), article 104198. https://doi.org/10.1016/j.jece.2020.104198

Article submitted: July 30, 2025: Peer review completed: October 5, 2025; Revised version received and accepted: March 3, 2026; Published: March 19, 2026.
DOI: 10.15376/biores.21.2.3954-3980